TWO APPROACHES UTILIZING INVARIANT MANIFOLDS TO DESIGN TRAJECTORIES FOR DMOC OPTIMIZATION

Ashley Moore

Invariant manifolds of the planar circular restricted 3-body problem are used to design initial guess trajectories from the Earth to the Moon which are then optimized using the optimal control algorithm DMOC (Discrete Mechanics and Optimal Control). The first approach focuses on patching invariant manifolds of the Sun-Earth and Earth-Moon 3-body systems together to create a trajectory in the 3-body problem and then modifying it to fit 4-body dynamics. The second approach selects endpoints on the manifolds near the Earth and Moon, and then locates intersections of trajectories originating at these endpoints in the 4-body problem directly. DMOC optimization of trajectories generated with the two methods generate very different trajectories while minimizing the necessary ΔV.

INTRODUCTION

Many techniques focus on the design of spacecraft trajectories. For example, invariant manifolds of the planar circular restricted 3-body problem (PCR3BP) can be used to find energy efficient trajectories that follow the natural dynamics of the solar system from one region of space to another. The 3-body problem is well understood and allows for the design of complicated trajectories not possible using patched conics. What about the design of a trajectory in the 4-body problem? Since the N-body problem is notoriously difficult to solve, much work has focused on patching multiple 3-body systems together, which typically include impulsive control at the intersection of the invariant manifolds of the two systems. The work of this project aims to extend this method, to solve the problem using 4-body dynamics and to apply local optimal control throughout the trajectory, instead of impulsive control concentrated at the intersection. Does the application of small ΔV throughout the trajectory, designed using an optimal control scheme, minimize the total ΔV? This project seeks to answer that question by combining invariant manifold techniques in the PCR3BP with the optimal control algorithm DMOC (Discrete Mechanics and Optimal Control) in two different ways.

Invariant Manifolds

Invariant manifolds are tube-like structures along which a spacecraft may travel using no energy. The manifolds can lead, for example, to periodic orbits around the Lagrange points of the PCR3BP. Conley (1968)[1] and McGeehee (1969)[2] were the first to study the orbit structures around the L_1 and L_2 Lagrange points. The transport made possible by invariant manifolds has been exploited for several different trajectories. For example, the work of Belbruno and Miller (1993)[3] presents the idea of patching these invariant manifold tubes together to effect transfer between the Earth and the Moon. Gómez et al. (1993)[4] studies transfer from the Earth to a Halo orbit about the L_1 equilibrium point of the Sun-Earth 3-body system. This project focuses on the trajectory studied in Koon et al. (2001 and 2000)[5,6] and Belbruno and Miller (1993)[3] which follows invariant manifolds to transfer from the Earth to the Moon.

Invariant manifold techniques usually only provide trajectories for uncontrolled spacecraft. Rather impulsive control is used at the intersection between different invariant manifolds. An extension of

invariant manifold techniques in order to account for a continuously applied control force is presented in Dellnitz et al. (2006)[7] and applied to design a trajectory from Earth to Venus and from Earth to L_2,[8] respectively. However, so far these techniques are only computationally reasonable for a constant one-dimensional control force. Instead we are interested in a time-dependent control law influencing all degrees of freedom of the spacecraft in each time point that are optimal w.r.t. a certain goal. Therefore, the application of a local optimal control scheme is indispensible for the design of trajectories with more complex control laws. Thereby, the computed thrustless trajectories designed with the help of invariant manifold techniques serve as initial guess for the optimization of the controlled model.

Local Optimal Control

The optimization for this project is performed using DMOC (*Discrete Mechanics and Optimal Control*) (Ober-Blöbaum (2008)[9] and Junge et al. (2005)[10]) which is based on the discretization of the variational structure of the mechanical system directly. The discretization of the Lagrange-d'Alembert principle[11] leads to structure preserving time stepping equations which serve as equality constraints for the resulting finite dimensional nonlinear optimization problem. This problem can be solved by standard nonlinear optimization techniques such as sequential quadratic programming (see e.g. Gill et al. (1997),[12] Gill et al. (2000),[13] Powell (1978)[14] and Han (1976)[15]).

Shoot the Moon

The Shoot the Moon problem, presented by Koon, Lo, Marsden and Ross,[6] computes a trajectory which begins in low Earth orbit, travels along the invariant manifolds of the Sun-Earth and Earth-Moon PCR3BPs, and ends in orbit about the Moon. Moore et al. (2009)[16] describes how the Shoot the Moon trajectory is modified to fulfill the dynamics of the 4-body problem and optimized using DMOC, reducing the ΔV. The DMOC results are locally optimal and very dependent on initial guess, so this project re-examines that work and explores a different way to design the initial guess trajectory. Two different initial guess trajectories are designed and then optimized using DMOC.

PROBLEM FORMULATION AND METHODS

The fundamental theory and the problem description that form the basis for this work are presented in this section including invariant manifolds of the planar restricted 3-body problem, the bicircular 4-body model, and DMOC.

Invariant Manifolds of the 3-Body Problem

The Shoot the Moon problem begins with two coupled planar circular restricted 3-body problems.[6] The geometry of the PCR3BP is shown in Figure 1. For each PCR3BP, the motion of a body is described under the influence of two main bodies, either the Sun and the Earth in the Sun-Earth system or the Earth and the Moon for the Earth-Moon system. Each system is described in a rotating coordinate frame and mass is normalized with the mass parameter

$$\mu = \frac{M_2}{M_1 + M_2} \tag{1}$$

where $M_1 > M_2$. For example, in the Sun-Earth 3-body system, M_1 denotes the mass of the Sun and M_2 denotes the mass of the Earth. The normalized mass of the larger body is denoted by

$m_1 = 1 - \mu$, and the normalized mass of the smaller body is $m_2 = \mu$. The two primary bodies rotate in circular, planar orbits about their common center of mass at the origin. The third body, the spacecraft, is assumed to have infinitesimal mass. The primary bodies, m_1 and m_2, are positioned at $(-\mu, 0)$ and $(1-\mu, 0)$, respectively. The equations of motion for the PCR3BP are

$$\ddot{x} - 2\dot{y} = \frac{\partial \Omega}{\partial x} \tag{2}$$

$$\ddot{y} + 2\dot{x} = \frac{\partial \Omega}{\partial y} \tag{3}$$

where

$$\Omega = \frac{x^2 + y^2}{2} + \frac{1-\mu}{\sqrt{(x+\mu)^2 + y^2}} + \frac{\mu}{\sqrt{(x-1+\mu)^2 + y^2}} \tag{4}$$

The system, Eq. (2)-(4), has five equilibrium points $L_1, \ldots, L_5$ (cf. Figure 1); the unstable L_2 point is of interest for this work.

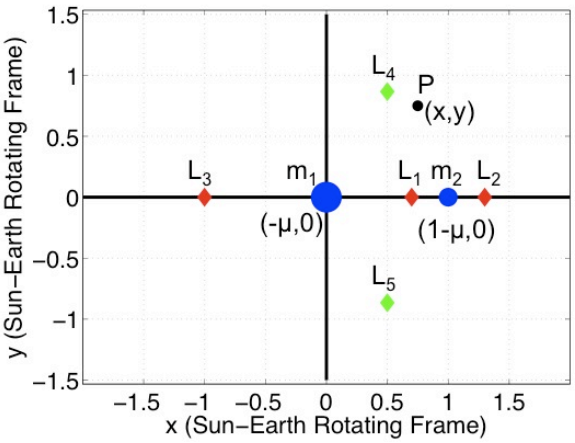

Figure 1 Geometry of PCR3BP in Sun-Earth rotating frame with two primary masses, m_1 and m_2, and Lagrange points $\{L_i\}_{i=1}^5$.

Stable and unstable manifolds emanate from the periodic orbit of the L_2 Lagrange point, shown in Figure 2. These manifold tubes control transport into and out of the region around m_2.[6] The unstable manifold of the Sun-Earth system leads away from the periodic orbit around L_2, while the stable manifold leads towards the periodic orbit.

The equations of motion for the PCR3BP are Hamiltonian and time independent, so there exists the following energy integral.

$$E = \frac{1}{2}(\dot{x}^2 + \dot{y}^2) - \Omega(x, y) \tag{5}$$

The phase space of the PCR3BP may be divided into regions of possible and forbidden motion based on this energy.[17] There are five possible cases, with the first four cases shown in Figure 3. Each plot shows the Hill's region, a projection of the energy surface $\mathcal{M}(\mu, e) = \{(x, y, \dot{x}, \dot{y}) | E(x, y, \dot{x}, \dot{y}) = e\}$ onto configuration space, for a particular energy level. The cases are distinguished by the critical energy $\{E_i\}_{i=1}^5$, which represents the energy of a particle at rest at the Lagrange point$\{L_i\}_{i=1}^5$. For example, if the energy of the spacecraft is greater than E_2 but less than E_3, it is energically possible for the spacecraft to move through the manifold tubes from the region surrounding m_2 to an exterior

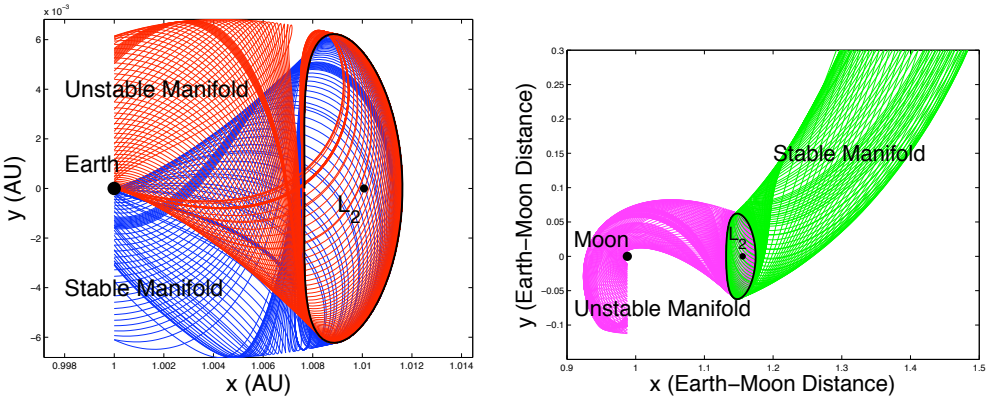

(a) (b)

Figure 2 Manifolds emanate from the periodic orbit about L_2 (a) Stable and Unstable manifolds of the Sun-Earth L_2 Lagrange point. (b) Stable and unstable manifolds of Earth-Moon L_2 Lagrange point.

region and vice versa, as shown in plot (c) of Figure 3. Furthermore, this energy is important for transfer between manifolds of different PCR3BPs.

Bicircular 4-Body Model

DMOC will optimize initial guess trajectories that obey the dynamics of the 4-body problem. The bicircular 4-body model describes the dynamics of the Sun, Earth, Moon, and spacecraft as follows. The Earth and Moon rotate in planar circular motion about their common center of mass. Then, the barycenter of the Earth-Moon system and the Sun rotate in planar circular motion about the common center of mass of the three bodies. As before, the mass of the spacecraft is negligible. Figure 4 shows the geometry of this 4-body model. The equations of motion for this model in Sun-Earth rotating coordinates are[17]

$$\ddot{x} - 2\dot{y} = \frac{\partial \Omega}{\partial x} \tag{6}$$

$$\ddot{y} + 2\dot{x} = \frac{\partial \Omega}{\partial y} \tag{7}$$

where

$$\Omega = \frac{x^2 + y^2}{2} + \frac{\mu_S}{\sqrt{(x - x_S)^2 + y^2}} + \frac{\mu_E}{\sqrt{(x - x_E)^2 + y^2}} + \frac{\mu_M}{\sqrt{(x - x_M)^2 + (y - y_M)^2}} \tag{8}$$

and μ_S, μ_E, and μ_M are the normalized mass of the Sun, Earth, and Moon, respectively, given by

$$\mu_S = 1 - \mu \tag{9}$$

$$\mu_E = \mu \tag{10}$$

$$\mu_M = \frac{M_M}{M_M + M_E + M_S} = 3.734 \cdot 10^{-8} \tag{11}$$

and

$$\mu = \frac{M_E + M_M}{M_E + M_M + M_S} = 3.036 \cdot 10^{-6} \tag{12}$$

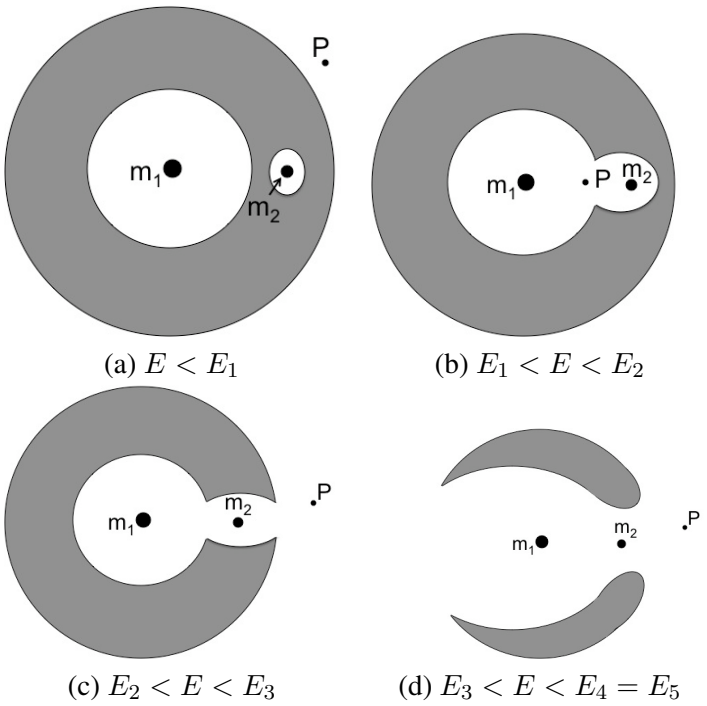

(a) $E < E_1$ (b) $E_1 < E < E_2$

(c) $E_2 < E < E_3$ (d) $E_3 < E < E_4 = E_5$

Figure 3 Regions of possible motion: (a) P cannot move between m_1 and m_2 (b) P can move between m_1 and m_2 via L_1 (c) P may move from m_1 to m_2 to exterior region via L_1 and L_2 (d) P may travel past m_1 to exterior region via L_3. Case 5, $E > E_5$, is not shown: P may move freely in x-y plane.

Note that M_i, $i = E, M, S$, denotes the body's mass in kg. Also, x_S, x_E, and x_M represent the x-position of the Sun, Earth, and Moon respectively, and y_M is the y-position of the Moon (the Sun and Earth lie on the x-axis). The position of the Moon is a function of time given by

$$\theta_M = \omega_M t + \theta_{M0} \tag{13}$$

$$x_M = a_M \cos\theta_M \tag{14}$$

$$y_M = a_M \sin\theta_M \tag{15}$$

where t is time, θ_{M0} is the initial angle of the Moon with respect to the x-axis in the Sun-Earth rotating frame, $a_M = 2.573 \cdot 10^{-3}$ is the normalized radius of the Moon's circular orbit, and $\omega_M = 12.369$ is the normalized rotation rate of the Moon.

Discrete Mechanics and Optimal Control

In order to compute a trajectory with minimal fuel consumption, we make use of local optimal control techniques. DMOC[10,9] is an optimal control scheme that is based on a direct discretization of the Lagrange-d'Alembert principle of the mechanical system. The discretization leads to the forced discrete Euler-Lagrange equations which are used as optimization constraints for a given cost function. The resulting restricted optimization problem is solved with an SQP solver.

Consider a mechanical system to be moved along a curve $q(t) \in Q$ during the time interval $t \in [0, T]$ from an initial state $(q^0, \dot{q}^0)$ to a final state $(q^T, \dot{q}^T)$ under the influence of a force $f(q(t), \dot{q}(t), u(t))$ where $u(t) \in U$ is a control parameter. The curves q and u are chosen to mini-

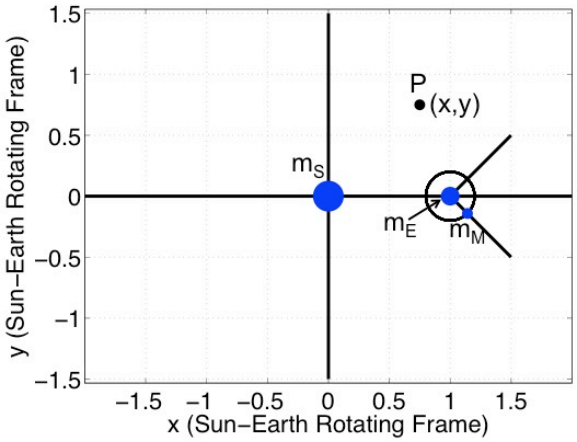

Figure 4 Bicircular 4-Body Model: geometry in the Sun-Earth rotating frame with three primary masses, m_S, m_E, and m_M, and spacecraft, P. The Moon rotates relative to the Sun-Earth rotating frame, which is stationary.

mize a given cost functional

$$J(q, \dot{q}, u) = \int_0^T C(q(t), \dot{q}(t), f(q(t), \dot{q}(t), u(t)))\, dt \tag{16}$$

subject to the condition that the system satisfies the Lagrange-d'Alembert principle, which states that

$$\delta \int_0^T L(q(t), \dot{q}(t))\, dt + \int_0^1 f(q(t), \dot{q}(t), u(t)) \cdot \delta q(t)\, dt = 0 \tag{17}$$

for all variations δq with $\delta q(0) = \delta q(T) = 0$, where $L : TQ \to \mathbb{R}$ is the Lagrangian consisting of the kinetic minus potential energy of the system.

The optimal control problem stated in Eq. (16) and Eq. (17) is now transformed into a finite dimensional constrained optimization problem using a global discretization of the states and the controls. We replace the state space TQ by $Q \times Q$ and consider the grid $\Delta t = \{t_k = kh \,|\, k = 0, \ldots, N\}$, $Nh = T$, where N is a positive integer and h the stepsize. We replace a path $q : [0, T] \to Q$ by a discrete path $q_d : \{t_k\}_{k=0}^N \to Q$, where we view $q_k = q_d(kh)$ as an approximation to $q(kh)$.[11,9] Similarly, we replace the control path $u : [0, T] \to U$ by a discrete one. To this end, we consider a refined grid $\Delta\tilde{t}$, generated via a set of control points $0 \le c_1 < \cdots < c_s \le 1$ as $\Delta\tilde{t} = \{t_{k\ell} = t_k + c_\ell h \,|\, k = 0, \ldots, N-1; \ell = 1, \ldots, s\}$. With this notation, the discrete control path is defined to be $u_d : \Delta\tilde{t} \to U$. We define the intermediate control samples u_k on $[t_k, t_{k+1}]$ as $u_k = (u_{k1}, \ldots, u_{ks}) \in U^s$ to be the values of the control parameters guiding the system from $q_k = q_d(t_k)$ to $q_{k+1} = q_d(t_{k+1})$, where $u_{kl} = u_d(t_{kl})$ for $l \in \{1, \ldots, s\}$.

Using an approximation of the action integral in Eq. (17) by a discrete Lagrangian $L_d : Q \times Q \to \mathbb{R}$,

$$L_d(q_k, q_{k+1}) \approx \int_{kh}^{(k+1)h} L(q(t), \dot{q}(t))\, dt$$

and discrete forces

$$f_k^- \cdot \delta q_k + f_k^+ \cdot \delta q_{k-1} \approx \int_{kh}^{(k+1)h} f(q(t), \dot{q}(t), u(t)) \cdot \delta q(t)\, dt$$

where the left and right discrete forces $f_k^{\pm}$ now depend on (q_k, q_{k+1}, u_k), we obtain the discrete Lagrange-d'Alembert principle, Eq. (18). Therefore, it is necessary to consider discrete paths $\{q_k\}_{k=0}^N$ such that for all variations $\{\delta q_k\}_{k=0}^N$ with $\delta q_0 = \delta q_N = 0$, it is true that

$$\delta \sum_{k=0}^{N-1} L_d(q_k, q_{k+1}) + \sum_{k=0}^{N-1} \left(f_k^- \cdot \delta q_k + f_k^+ \cdot \delta q_{k+1} \right) = 0 \tag{18}$$

In the same manner, we obtain via an approximation of the cost functional Eq. (16), discrete cost functions C_d and J_d, respectively.

Then, the goal of the discrete constrained optimization problem is to minimize the discrete cost function

$$J_d(q_d, u_d) = \sum_{k=0}^{N-1} C_d(q_k, q_{k+1}, u_k) \tag{19}$$

subject to the constraints

$$\begin{aligned}
q_0 &= q^0 && (20)\\
q_N &= q^T && (21)\\
D_2L(q^0, \dot{q}^0) + D_1L_d(q_0, q_1) + f_0^- &= 0 && (22)\\
D_2L_d(q_{k-1}, q_k) + D_1L_d(q_k, q_{k+1}) + f_{k-1}^+ + f_k^- &= 0 && (23)\\
-D_2L(q^T, \dot{q}^T) + D_2L_d(q_{N-1}, q_N) + f_{N-1}^+ &= 0 && (24)
\end{aligned}$$

with $k = 1, ..., N-1$. The first two constraints require that the initial and final discrete positions match the continuous positions. The third and final constraints are the discrete momentum boundary conditions, and the fourth condition is the forced discrete Euler-Lagrange equation resulting from Eq. (18). Balancing accuracy and efficiency, we approximate the discrete cost function, C_d, the discrete Lagrangian, L_d, and the discrete forces with the midpoint rule and assume constant control parameters on each time interval with $l = 1$ and $c_1 = \frac{1}{2}$ as

$$C_d(q_k, q_{k+1}, u_k) = hC\left(\frac{q_{k+1} + q_k}{2}, \frac{q_{k+1} - q_k}{2}, u_k\right) \tag{25}$$

$$L_d(q_k, q_{k+1}) = hL\left(\frac{q_{k+1} + q_k}{2}, \frac{q_{k+1} - q_k}{h}\right) \tag{26}$$

$$f_k^- = f_k^+ = \frac{h}{2} f\left(\frac{q_{k+1} + q_k}{2}, \frac{q_{k+1} - q_k}{2}, u_k\right) \tag{27}$$

Eq. (19)-(24) describe a nonlinear optimization problem with equality constraints, which can be solved by standard optimization methods like SQP. Optionally, we can also include inequality constraints on states and controls.

TRAJECTORY DESIGN USING INVARIANT MANIFOLDS

This project focuses on two different methods that use invariant manifolds for trajectory design. Method 1, detailed in Moore et al. (2009),[16] utilizes the unstable Sun-Earth manifold and the stable Earth-Moon manifold and begins by designing a trajectory in the 3-body problem before modifying it for the 4-body problem. Method 2 focuses on the stable Sun-Earth manifold and the unstable Earth-Moon manifold and directly generates a trajectory in the 4-body problem.

Method 1

To achieve transfer between the Earth and Moon using the invariant manifolds, the first step is to locate the intersection of the unstable Sun-Earth manifold with the stable Earth-Moon manifold. A Poincaré section is used to find this intersection in the Sun-Earth rotating frame. The phase of the Earth-Moon frame with respect to the Sun-Earth frame can be adjusted until a suitable intersection is found.

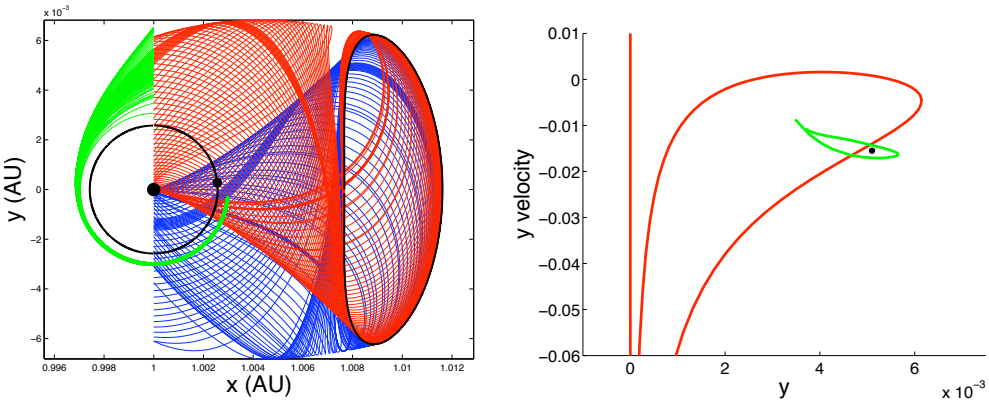

(a) Manifolds (b) Poincaré Section

Figure 5 (a) Intersecting Earth-Moon and Sun-Earth manifolds in Sun-Earth rotating coordinates. (b) Poincaré section showing the intersection of the stable Earth-Moon manifold with the unstable Sun-Earth manifold. The patch point is chosen inside stable Earth-Moon manifold and outside the unstable Sun-Earth manifold.

Using the Poincaré section, shown on the right hand side of Figure 5, a patch point is selected that falls within the stable manifold of the Earth-Moon system and outside the unstable manifold of the Sun-Earth system. From the Poincaré section, the patch point includes x, y, and $\dot{y}$. The x-velocity, $\dot{x}$, is selected so that the energy integral at the patch point equals that of the desired manifold. Forward integration of the conditions at the patch point (x, y, $\dot{x}$, $\dot{y}$) leads to a trajectory that flows through the stable Earth-Moon manifold and ends near the Moon. The same initial conditions are modified slightly in $\dot{x}$ and $\dot{y}$ and integrated backwards, generating a trajectory that hugs the unstable Sun-Earth manifold and then twists, targeting back to the Earth. The modification in the velocity ensures that the energy of the spacecraft is at the appropriate level to travel along the Sun-Earth manifold in the desired manner. The Sun-Earth and Earth-Moon trajectories are patched together to form a trajectory which begins at the Earth and ends at the Moon. Note that at the patch point, the energy is discontinuous; therefore, a ΔV is necessary to jump from the energy level of the Sun-Earth manifold to the energy of the Earth-Moon manifold. For mathematical details about this process, we refer to Koon et al. (2001)[6] and Ross (2004).[17] The trajectory is shown in Figure 6; it begins in an 315 km radius circular orbit about the Earth and ends in an $3.82 \cdot 10^5$ km circular orbit about the Moon. An initial thrust of 3,246.9 m/s is required to escape Earth orbit along the trajectory, a mid-course ΔV of 124.3 m/s is applied at the patch point, and a final ΔV of 3,024.0 m/s is required to settle into a permanent circular orbit at the Moon.

Now we want to modify this trajectory to fulfill the dynamics of the 4-body problem. Beginning with the same initial conditions from the patch point, $\dot{x}$ and $\dot{y}$ are modified slightly and integrated using the bicircular 4-body model. The modification is necessary due to the differences between the dynamics of the PCR3BP and the bicircular 4-body problem. The point is modified differently

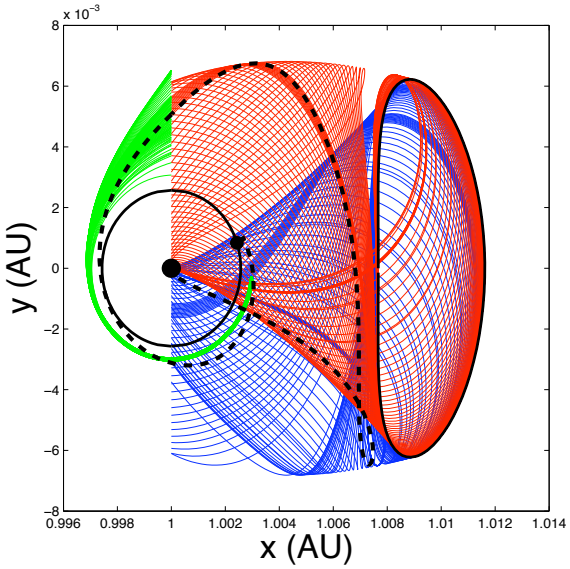

Figure 6 Trajectory in 3-body problem (in Sun-Earth Rotating coordinates): begins near the Earth, hugs the Sun-Earth unstable manifold towards the periodic orbit of L_2. It twists and then intersects the stable manifold of the Earth-Moon system, following that manifold to the realm of the Moon.

for the Sun-Earth section and the Earth-Moon section because of the energy differences between the manifolds of the two systems. Thus, the initial conditions denoted by IC_{SE} and IC_{EM}, respectively, can be expressed as

$$IC_{SE} = \left[\begin{array}{cccc} x & y & \dot{x} + \Delta\dot{x}_{SE} & \dot{y} + \Delta\dot{y}_{SE} \end{array} \right] \quad (28)$$

$$IC_{EM} = \left[\begin{array}{cccc} x & y & \dot{x} + \Delta\dot{x}_{EM} & \dot{y} + \Delta\dot{y}_{EM} \end{array} \right] \quad (29)$$

IC_{SE} is integrated backwards to generate the Sun-Earth portion of the trajectory, and IC_{EM} is integrated forwards to generate the Earth-Moon portion of the trajectory. Note that the Δ's are adjusted until a good trajectory is found: a trajectory which begins and ends at a desired radius about the Earth and Moon, respectively. Note that the initial and final momentum values may not be favorable. DMOC adjusts these momentum values according to the specified constraints and cost function during optimization. This trajectory serves as the initial guess for DMOC, IG1.

Method 2

To design a trajectory valid for the 4-body problem, start with the unstable Earth-Moon manifold and stable Sun-Earth manifold. Select an end point on each manifold a desired distance from the Moon and Earth, respectively. For example, IC_M is selected such that the distance from the Moon is 554.5 km, and IC_E gives a distance from the Earth of 210 km. Now integrate the conditions at IC_M (transformed from Earth-Moon rotating coordinates to Sun-Earth rotating coordinates) and IC_E backwards and forwards, respectively, in the 4-body problem to generate Traj_M and Traj_E. Figure 7(a) shows Traj_M transformed back to Earth-Moon rotating coordinates, and Figure 7(b) shows Traj_E.

Next, find the intersection of the resulting trajectories - this is the patch point, shown in Figure 7(c). Using the conditions of Traj_M at the patch point, integrate forwards in the 4-body problem

to create Traj$_{M2}$ (identical to Traj$_M$, but it flows in the opposite direction, towards the Moon instead of away from it). Note that even though the trajectories intersect in x-y space, they don't actually intersect in time. Therefore, the Moon is in a different position for Traj$_M$ and Traj$_E$. This is a problem. So, the conditions of Traj$_E$ at the patch point are modified slightly and integrated using a consistent Moon position to give Traj$_{E2}$, which is similar to Traj$_E$ and ends in the desired location. Figure 7 shows the trajectory combining Traj$_{M2}$ and Traj$_{E2}$ joined by an impulsive force at the patch point.

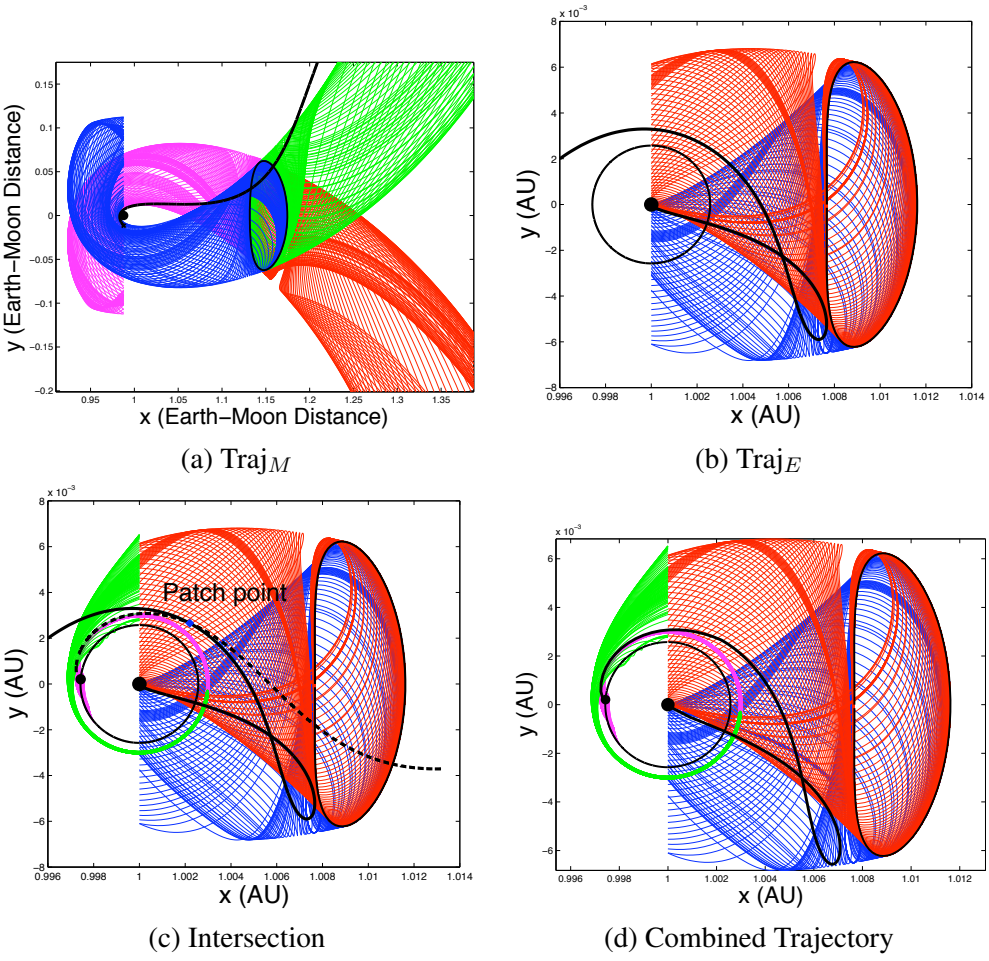

(a) Traj$_M$ (b) Traj$_E$

(c) Intersection (d) Combined Trajectory

Figure 7 Process for method 2: (a) Integrate point on Earth-Moon unstable manifold backwards in 4-body problem. (b) Integrate point on Sun-Earth stable manifold forwards in 4-body problem. (c) Locate intersection of the two trajectories (d) Connect the trajectories.

OPTIMIZATION PROCEDURE

The optimization method can be broken into three parts: creation of the initial guess trajectory in the 4-body problem, computation of a feasible trajectory, and DMOC optimization. Each step of the process is performed using *Matlab*, and the SQP solver *fmincon* runs the optimization.

Creation of Initial Guess

For an initial guess trajectory, we use a constant step size between nodes for DMOC. However, the nonlinearity of the dynamics poses a problem. If a single step size is used throughout the trajectory, two scenarios are possible. First, if a medium step size is used, e.g. $\mathcal{O}(10^{-2})$, there are not enough nodes near the Earth and Moon to accurately capture the dynamics. On the other hand, if a sufficiently small step size is used, e.g. $\mathcal{O}(10^{-5})$, there are too many nodes for a reasonable computation time. To solve this problem, the trajectory is broken into m separate sections of uniform step size h_i with discrete paths $(q_i)_d$ and discrete control paths $(u_i)_d$, $i = 1, \ldots, m$. Then, when DMOC is applied, the position and velocity at the boundaries are enforced as additional constraints for the optimization problem. For example, the position and velocity of the final node of section 1 must equal that of the first node of section 2. Four sections are chosen as the ideal number to capture the dynamics in the fewest number of nodes. Figure 8 shows IG1, the initial guess trajectory created using method 1 with sections. The step sizes for IG1 are $h_1 = 1 \cdot 10^{-5}$, $h_2 = 2 \cdot 10^{-3}$, $h_3 = 2 \cdot 10^{-2}$, $h_4 = 1 \cdot 10^{-4}$, respectively.

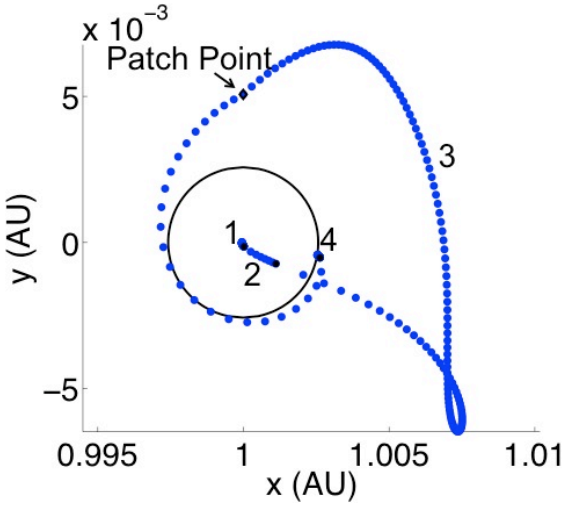

Figure 8 Sections of guess for Method 1. The trajectory is divided into four sections of uniform step size ensuring that the trajectory consists of sufficient nodes near the Earth and Moon to capture the dynamics but few enough total nodes for reasonable computation time using *Matlab*.

This initial guess created using method 1 is called IG1. An initial guess with sections is also generated using method 2, termed IG2. Both trajectories are plotted in Figure 9, demonstrating the differences between the two trajectories. IG2 takes roughly half the time to reach the Moon compared to IG1, and the final position of the Moon is different for the two trajectories. Table 1 displays the trajectory details including initial altitude at the Earth, final altitude at the Moon, the total ΔV which is broken into: ΔV_E (the ΔV necessary to leave circular Earth orbit), ΔV_M (the ΔV necessary to inject the spacecraft into a circular orbit at the Moon), ΔV_{traj} (the ΔV applied at the patch point), and the number of nodes. Figure 10 shows the control magnitude for IG1 and IG2, demonstrating the impulsive nature of the ΔV.

Table 1. Details of Initial Guess Trajectories

	IG1	IG2
Initial Earth Orbit Altitude (km)	207	210
Final Moon Orbit Altitude (km)	326.8	554.5
Time of Flight (days)	175	96.9
Total ΔV (m/s)	5,305.9	9,065.1
ΔV_E (m/s)	3,216.0	7,817.5
ΔV_M (m/s)	1,943.5	1,056.1
ΔV_{traj} (m/s)	146.4	191.5
Number of nodes	271	489

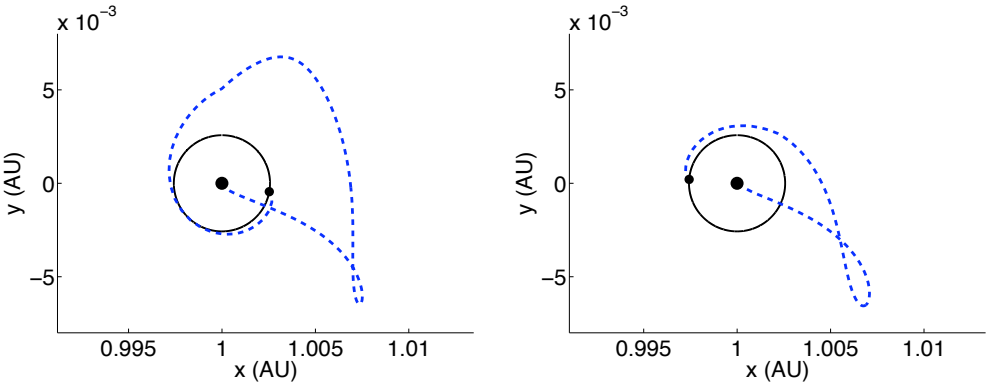

(a) IG1 (b) IG2

Figure 9 Initial guess trajectories: (a) Initial guess created using method 1. (b) Initial guess created using method 2.

Feasible Trajectories

For DMOC, the state q includes (x, y) and represents the x- and y-position of the trajectory. The Lagrangian describing the bicircular 4-body model is

$$L = \frac{1}{2}\left(\dot{x}^2 + \dot{y}^2\right) + \frac{1}{2}\left(x^2 + y^2\right) + x\dot{y} - y\dot{x} + \frac{\mu_E}{\sqrt{(x - x_E)^2 + y^2}} + \frac{\mu_S}{\sqrt{(x - x_S)^2 + y^2}} + \frac{\mu_M}{\sqrt{(x - x_M)^2 + (y - y_M)^2}} \tag{30}$$

The control force, $f(q, \dot{q}, u) = u$, consisting of the control parameters (u_x, u_y) represents the control force in the x- and y-direction, respectively. The next step before the optimization is the formulation of a feasible trajectory. By definition, a feasible trajectory is a solution that satisfies the dynamics of the system and desired boundary conditions but is not optimal. To create a feasible trajectory, DMOC is applied with the cost function set to one, allowing DMOC to adjust the optimization variables to fulfill the constraints. The constraints require that the forced discrete Euler-Lagrange equations, derived from the above Lagrangian, are fulfilled (enforcing the dynamics), the initial and final radius about the Earth and Moon, respectively, must match the initial guess. Also, the initial and final radial velocity must be zero. This constraint reduces the ΔV_E and ΔV_M.

Note that even though IG1 and IG2 both have impulsive control applied at the patch point, when input into DMOC, the control force is assumed to be zero throughout the trajectory. This allows

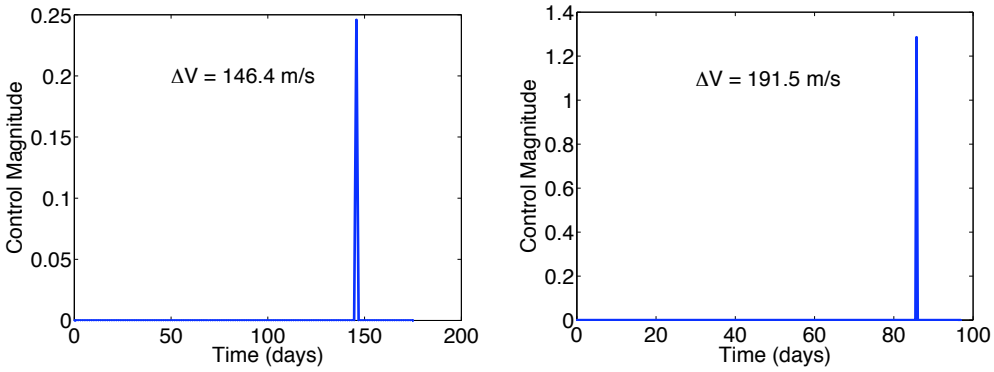

(a) IG1 Control Magnitude (b) IG2 Control Magnitude

Figure 10 Initial guess control magnitude: (a) Control magnitude for IG1. (b) Control magnitude for IG2.

DMOC to find a smooth control profile that fulfills the Euler-Lagrange equations. If the impulsive force is included, DMOC returns a control profile with an impulse and much higher ΔV. Figure 11 shows the feasible trajectories, and Figure 12 shows the time evolution of the control magnitude $U = \sqrt{u_x^2 + u_y^2}$, for each trajectory. Note that the control profile does not include ΔV_E and ΔV_M. Table 2 displays the flight time and ΔV for each of the feasible trajectories.

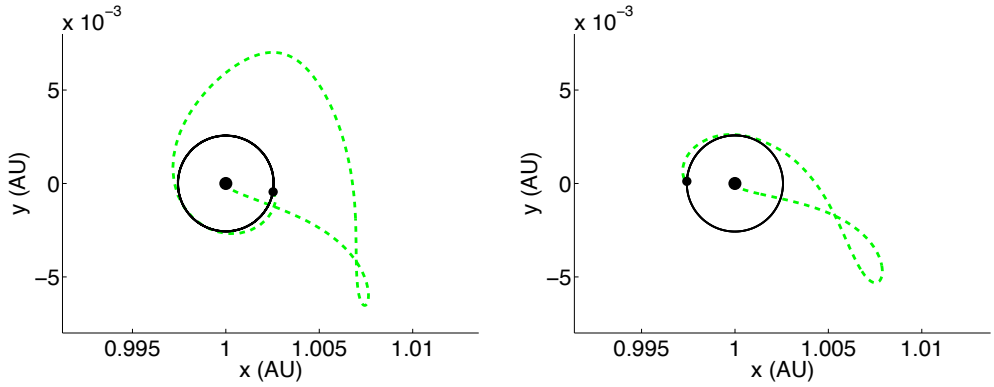

(a) Feasible 1 (b) Feasible 2

Figure 11 DMOC feasible trajectories: (a) Feasible trajectory for IG1. (b) Feasible trajectory for IG2.

Optimization

Now, the feasible trajectories are used as initial guesses for the full DMOC optimization. For optimization, the discrete cost function is

$$J_d(u_d) = h_1\|(u_1)_d\|^2 + h_2\|(u_2)_d\|^2 + h_3\|(u_3)_d\|^2 + h_4\|(u_4)_d\|^2 \tag{31}$$

where $(u_i)_d = \{(u_{x,i}, u_{y,i})_k\}_{k=0}^{N_i-1}$ is a vector of length $2N_i$ with $N_i + 1$ being the number of discretization points in section i, $i = 1, \ldots, 4$, $\|\cdot\|$ denotes the 2-norm. The ΔV applied throughout the trajectory, based on the control forces computed with DMOC, is computed as follows:

$$\Delta V_{traj} = \alpha_V \left(h_1\|(u_1)_d\| + h_2\|(u_2)_d\| + h_3\|(u_3)_d\| + h_4\|(u_4)_d\|\right) \tag{32}$$

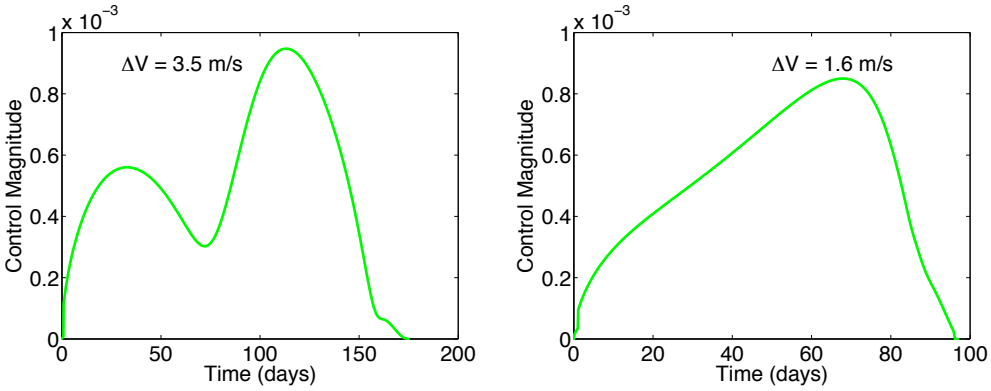

(a) Feasible Control Magnitude 1 (b) Feasible Control Magnitude 2

Figure 12 DMOC feasible control magnitude: (a) Feasible control magnitude for IG1. (b) Feasible control magnitude for IG2.

Table 2. Details of Feasible Trajectories

	Feasible 1	Feasible 2
Flight Time (days)	175	96.6
Total ΔV (m/s)	3,567.3	3,822.0
ΔV_E (m/s)	2,931.4	3,201.0
ΔV_M (m/s)	632.4	619.4
ΔV_{traj} (m/s)	3.5	1.6

where α_V scales the velocity to m/s units. The constraints are the same as for the feasible trajectories.

OPTIMIZATION RESULTS

DMOC is run using the feasible trajectories Feasible 1 and Feasible 2 as initial guesses, leading to the locally optimal trajectories Optimal 1 and Optimal 2, respectively. The trajectories are shown in Figure 13, the control magnitudes, excluding ΔV_E and ΔV_M, are shown in Figure 14, and the flight time and ΔV are shown in Table 3.

Table 3. Details of Optimal Trajectories

	Optimal 1	Optimal 2
Flight Time (days)	175	96.9
Total ΔV (m/s)	3,566.8	3,823.3
ΔV_E (m/s)	2,931.5	3,200.9
ΔV_M (m/s)	632.4	621.8
ΔV_{traj} (m/s)	2.9	0.6

Comparison of the DMOC optimal results with the initial guess trajectories clearly displays DMOC's power. While IG1 requires an impulsive ΔV_{traj} of 146.4 m/s to travel from the Earth to the Moon, DMOC generates a trajectory requiring just 2.9 m/s. DMOC also reduces the ΔV necessary to leave and enter circular orbits at the given start and end positions (ΔV_E and ΔV_M). Optimization of IG2 yields even better results with a reduction of ΔV_{traj} from 191.5 m/s to just 0.6 m/s.

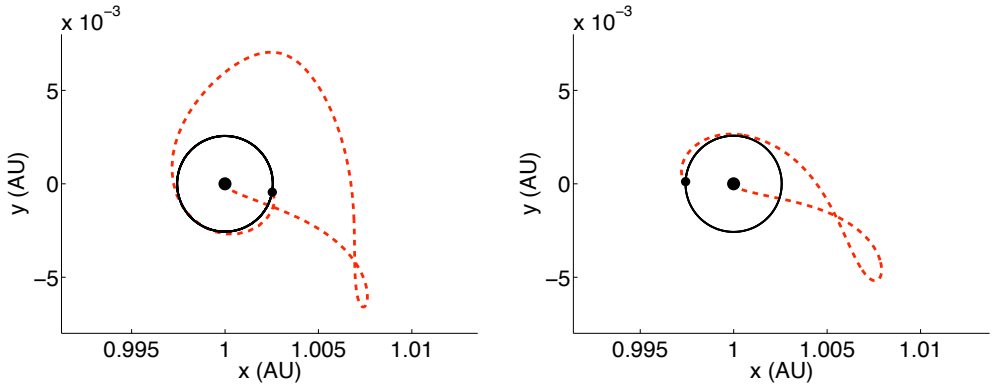

(a) Optimal 1 (b) Optimal 2

Figure 13 DMOC optimal trajectories: (a) Optimal trajectory for IG1. (b) Optimal trajectory for IG2.

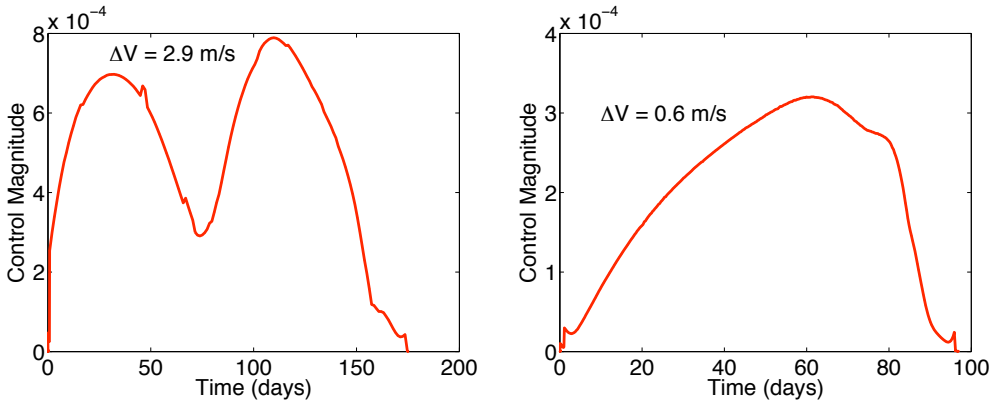

(a) Optimal Control Magnitude 1 (b) Optimal Control Magnitude 2

Figure 14 DMOC optimal control magnitude: (a) Optimal control magnitude for IG1. (b) Optimal control magnitude for IG2.

As shown in Figure 14, the optimal control magnitude is slightly more jagged than the corresponding feasible control magnitude, Figure 12. The cause is unknown at this time. However, upon close examination of both optimal and feasible control magnitude, small discontinuities occur in the control at the section boundaries. These discontinuities are the result of the change in step size at the boundary.

Further examination of the optimal control magnitude reveals very small oscillation for section 1 at the beginning of the trajectory, shown in Figure 15 for Optimal Control Magnitude 1. This oscillation occurs in the optimal control in section 1 for both methods 1 and 2. However, the control magnitude for sections 2-4 is fairly smooth and continuous. In the Euler-Lagrange equations, the discrete control force appears as $\frac{h \cdot u}{2}$, and for section 1, that quantity is less than the tolerance of the algorithm. As far DMOC is concerned, the control force for that section is effectively zero, despite the oscillation that is seen in the figure. Clearly, a higher tolerance value is needed, but experience demonstrates that DMOC struggles to converge for tolerances smaller than 10^{-11}, the value used to obtain the result shown in Figure 15. Note that this oscillation does not occur for the control magnitude of the feasible trajectories.

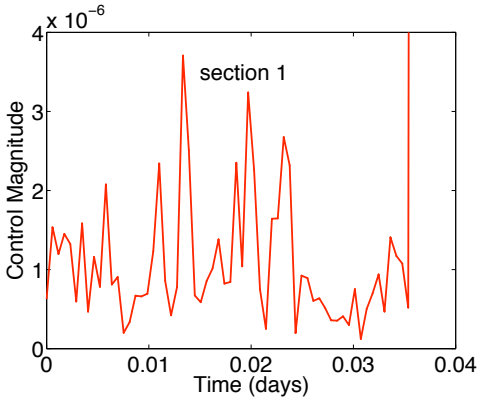

Figure 15. Control magnitude for section 1 of Optimal 1

It is useful to compare the initial guess, feasible, and optimal trajectories on one plot. As shown in Figure 16, the optimal and feasible trajectories are very similar for both method 1 and 2. For method 1, the feasible and optimal trajectories smooth out the kink at the patch point. The trajectories generated by methods 1 and 2 are optimized using identical Euler-Lagrange equations and very similar constraints, and the vast difference between the results demonstrates the local nature of DMOC optimization. This point is further emphasized when comparing the variable time results from Moore et al. (2009)[16] with the results of method 2. It is possible to add an additional variable that allows DMOC to adjust the final time, which adjusts the final position of the Moon. Optimization of IG1 with the flight time included in the cost function leads to trajectory results very similar to Optimal 1 with a smaller ΔV_M, but the flight time is reduced by less than a day. Using method 2, the flight time is nearly 80 days less than the trajectory generated with method 1. Therefore, even though DMOC strives to minimize the flight time, without an appropriate initial guess, it finds only a local minimum.

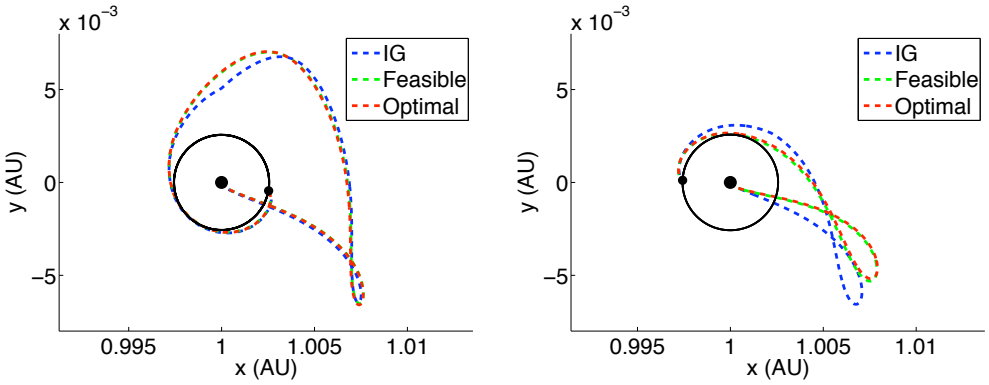

Figure 16 Comparison of initial guess, feasible, and optimal trajectories for: (a) method 1 (b) method 2

Additionally, the chosen cost function can lead to very different control results. In Moore et al.

(2009),[16] the following cost function is used.

$$J_d(u_d) = h_1\|(u_1)_d\| + h_2\|(u_2)_d\| + h_3\|(u_3)_d\| + h_4\|(u_4)_d\| \tag{33}$$

Optimization of the Feasible 1 trajectory using this cost function, results in a trajectory very similar to Optimal 1 shown in Figure 13(a), but the resulting control profile is very different. As shown in Figure 17, the control is not continuous and the magnitude is larger. In fact, the optimal ΔV of 6.6 m/s is actually larger than the feasible ΔV of 3.5 m/s. This result demonstrates the importance of a proper cost function.

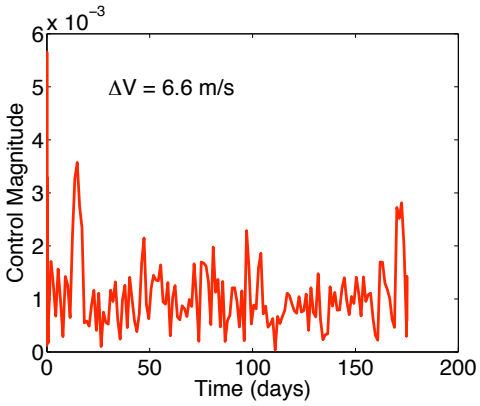

Figure 17. DMOC optimal control magnitude for different cost function.

CONCLUSION AND FUTURE WORK

Invariant manifolds may be used in two different ways to design trajectories for DMOC optimization, as demonstrated by methods 1 and 2. The optimized trajectories of both methods greatly reduce not only the ΔV throughout the trajectory, but also the ΔV necessary to leave and enter circular orbit at the endpoints. The vastly different results of the two methods clearly demonstrate the local nature of DMOC and the possibility that there exists a globally optimal solution. Also, the new cost function, $J_d = h||u||^2$, yields much better results than the cost function previously used, $J_d = h||u||$. Finally the results reveal some interesting artifacts of the discretization and a need for further error analysis.

For the shoot the moon problem, an adaptive time-stepping strategy for DMOC would provide a huge benefit and is also essential for other problems in space mission design, e.g. the trajectories require a finer time-stepping near planets due to the strong influence of gravity, while for a transfer in nearly free space, only a few discretization points are necessary to accurately reflect the dynamics of the system. Here, different strategies such as error control based on the discretization grid under consideration[18] and variational approaches[19] could be investigated.

In addition, since DMOC results are locally optimal, dependent on initial guess, further investigation leading to globally optimal solutions is desirable. Kobilarov (2008)[20] combines DMOC with sampling-based roadmaps to compute near globally optimal solutions for various problems including a helicopter traveling through an urban environment towards a goal state. This motion planning method begins by compiling a library of DMOC primitives (short, optimal paths from a start state to an intermediate goal state). Then, a sampling-based roadmap strategy (e.g. probabilistic roadmaps) combines these DMOC primitives into a full trajectory that reaches the goal state.

The use of DMOC primitives depends on the invariance of the dynamics under some group action.[20] Due to the time-dependent nature of the dynamics of the 4-body problem, DMOC primitives most likely will not be applicable for this problem. However, a similar strategy may successfully lead to globally optimal trajectories in the 4-body problem. One idea is to apply probabilistic roadmaps to create a mesh along the state space of the invariant manifolds of the PCR3BP, and then DMOC will be used to connect points on the mesh from the start state to goal state, minimizing the necessary control.

ACKNOWLEDGMENT

The author would like to acknowledge Dr. Shane Ross for his help with the Shoot the Moon problem and invariant manifolds, Dr Sina Ober-Blöbaum for indispensable DMOC guidance, and Dr. Jerrold E. Marsden, Dr. Marin Kobilarov, Stefano Campagnola, and Evan Gawlik for many useful discussions.

REFERENCES

[1] C. Conley, "Low Energy Transit Orbits in the Restricted Three-Body Problem," *SIAM J. Appl. Math*, Vol. 16, 1968, pp. 732–746.

[2] R. McGehee, *Some Homoclinic Orbits for the Restricted Three-Body Problem*. PhD thesis, University of Wisconsin, 1969.

[3] E. A. Belbruno and J. Miller, "Sun-perturbed Earth-to-Moon Transfers with Ballistic Capture," *Journal of Guidance, Control, and Dynamics*, Vol. 16, No. 4, 1993, pp. 770–775.

[4] G. Gómez, A. Jorba, J. Masdemont, and C. Simó, "Study of the Transfer From the Earth to a Halo Orbit Around the Equilibrium Point L_1," *Celestial Mechanics and Dynamical Astronomy*, Vol. 56, 1993, pp. 541–562.

[5] W. S. Koon, M. W. Lo, J. E. Marsden, and S. D. Ross, "Low Energy Transfer to the Moon," *Celestial Mechanics and Dynamical Astronomy*, Vol. 81, No. 1-2, 2001, pp. 63–73.

[6] W. S. Koon, M. W. Lo, J. E. Marsden, and S. D. Ross, "Shoot the Moon," *Spaceflight Mechanics*, Vol. 105, No. 2, 2000, pp. 1017–1030.

[7] M. Dellnitz, S. Ober-Blöbaum, M. Post, O. Schütze, and B. Thiere, "A Multi-objective Approach to the Design of Low Thrust Space Trajectories Using Optimal Control," Submitted to *Celestial Mechanics and Dynamical Astronomy*, 2008.

[8] M. Dellnitz, O. Junge, M. Post, and B. Thiere, "On Target for Venus—Set Oriented Computation of Energy Efficient Low Thrust Trajectories," *Celestial Mechanics & Dynamical Astronomy.*, Vol. 95, No. 1-4, 2006, pp. 357–370.

[9] S. Ober-Blöbaum, *Discrete Mechanics and Optimal Control*. PhD thesis, University of Paderborn, 2008.

[10] O. Junge, J. E. Marsden, and S. Ober-Blöbaum, "Discrete Mechanics and Optimal Control," *Proceedings of the 16th IFAC World Congress*, 2005.

[11] J. E. Marsden and M. West, "Discrete Mechanics and Variational Integrators," *Acta Numerica*, Vol. 10, 2001, pp. 357–514.

[12] P. E. Gill, W. Murray, and M. A. Saunders, "SNOPT: An SQP Algorithm for Large-scale Constrained Optimization," Report NA 97-2, Department of Mathematics, University of California, San Diego, CA, USA, 1997.

[13] P. E. Gill, L. O. Jay, M. W. Leonard, L. R. Petzold, and V. Sharma, "An SQP Method for the Optimal Control of Large-scale Dynamical Systems," *J. Comp. Appl. Math*, Vol. 20, 2000, pp. 197–213.

[14] M. J. D. Powell, "A Fast Algorithm for Nonlinearly Constrained Optimization Calculations," *Numerical Analysis* (G. A. Watson, ed.), Vol. 630 of *Lecture Notes in Mathematics*, pp. 261–280, Springer, 1978.

[15] S. P. Han, "Superlinearly Convergent Variable-metric Algorithms for General Nonlinear Programming Problems," *Mathematical Programming*, Vol. 11, 1976, pp. 263–282.

[16] A. Moore, S. Ober-Blöbaum, and J. E. Marsden, "Optimization of spacecraft trajectories: a method combining invariant manifold techniques and discrete mechanics and optimal control," *AAS Space Flight Mechanics Meeting*, Savannah, Georgia, AAS, 2009.

[17] S. D. Ross, *Cylindrical Manifolds and Tube Dynamics in the Restricted Three-Body Problem*. PhD thesis, California Institute of Technology, 2004.

[18] J. T. Betts, "Survey of Numerical Methods for Trajectory Optimization," *AIAA J. Guidance, Control, and Dynamics*, Vol. 21, No. 2, 1998, pp. 193–207.

[19] L. Kharevych, P. Mullen, S. Leyendecker, Y. Tong, J. E. Marsden, and M. Desbrun, "Robust Time-adaptive Integrators for Computer Animation," In preparation, 2008.

[20] M. Kobilarov, *Discrete Geometric Motion Control of Autonomous Vehicles*. PhD thesis, University of Southern California, August 2008.